

Analyzing the Error of Generative Diffusion Models: From Euler-Maruyama to Higher-Order Schemes*

Emanuel Pfarr[†] Radu Timofte[‡] Frank Werner[§]

January 27, 2026

Abstract

Although generative diffusion models (GDMs) are widely used in practice, their theoretical foundations remain limited, especially concerning the impact of different discretization schemes applied to the underlying stochastic differential equation (SDE). Existing convergence analysis largely focuses on Euler–Maruyama (EM)-like methods and does not extend to higher-order schemes, which are naturally expected to provide improved discretization accuracy. In this paper, we establish asymptotic 2-Wasserstein convergence results for SDE-based discretization methods employed in sampling for GDMs. We provide an all-at-once error bound analysis of the EM method that accounts for all error sources and establish convergence under all prevalent score-matching error assumptions in the literature, assuming a strongly log-concave data distribution. Moreover, we present the first error bound result for arbitrary higher-order SDE-discretization methods with known strong L_2 convergence in dependence on the discretization grid and the score-matching error. Finally, we complement our theoretical findings with an extensive numerical study, providing comprehensive experimental evidence and showing that, contrary to popular believe, higher order discretization methods can in fact retain their theoretical advantage over EM for sampling GDMs.

1 Introduction

Since their introduction in [24], generative diffusion models (GDMs) have become state-of-the-art across a wide range of generation tasks and now power major commercial text-to-image systems such as DALL·E. A well-known drawback of diffusion models, particularly compared to other prevalent generative approaches such as generative adversarial networks, is their slow and computationally expensive inference procedure. As a consequence, accelerating the generation process in diffusion models has become an active

*This work was partially supported by the Alexander von Humboldt Foundation.

[†]Institute of Mathematics, Julius-Maximilians-Universität Würzburg, Würzburg, Germany (emanuel.pfarr@uni-wuerzburg.de)

[‡]Center for Artificial Intelligence and Data Science, Julius-Maximilians-Universität Würzburg, Würzburg, Germany (radu.timofte@uni-wuerzburg.de)

[§]Institute of Mathematics, Julius-Maximilians-Universität Würzburg, Würzburg, Germany (frank.werner@uni-wuerzburg.de).

area of research. The reformulation of diffusion models as stochastic differential equations (SDEs) in [25] clarified that improving inference speed is fundamentally a matter of simulating the underlying SDE more efficiently. Moreover, since these SDEs do not admit closed-form solutions, faster simulation naturally suggests the use of more accurate or higher-order numerical discretization methods. Surprisingly, several works (e.g., [15, 14]) have shown that applying standard higher-order solvers “out of the box” often yields worse-than-expected performance compared to wide spread, low order discretization methods such as the classical Euler–Maruyama method or GDM specific discretizations.

1.1 Background

Generative diffusion models [25] consist of two parts. The so called forward process connects an unknown data distribution \mathcal{P}_0 on \mathbb{R}^d to a standard Gaussian distribution through a forward SDE

$$dx_t = a(t, x_t) dt + b(t, x_t) dW_t, \quad x_0 \sim \mathcal{P}_0. \quad (1)$$

Here, the drift $a : [0, \infty) \times \mathbb{R}^d \rightarrow \mathbb{R}^d$ and the diffusion coefficient $b : [0, \infty) \times \mathbb{R}^d \rightarrow \mathbb{R}^{d \times d}$ are carefully chosen functions to ensure $\lim_{t \rightarrow \infty} x_t \stackrel{D}{=} \mathcal{N}(0, \sigma^2 I_d)$ with a known constant $\sigma^2 \in \mathbb{R}$ and the d -dimensional unit matrix I_d . The second part of generative diffusion models, the so called backward process, is used to actually generate samples from the data distribution \mathcal{P}_0 . It consists of simulating the reverse-time SDE of the forward process eq. (1). Using classical time-reversal results [1, 12], the reverse-time dynamics are given by

$$dy_t = [-a(\tau, y_t) + b^2(\tau, y_t) s(\tau, y_t)] dt + b(\tau, y_t) dW_t, \quad y_0 \sim \mathcal{L}(x_T), \quad (2)$$

with $\tau = T - t$, the law $\mathcal{L}(x_T)$ of the random variable x_T and the so called *score function*: $s : [0, \infty) \times \mathbb{R}^d \rightarrow \mathbb{R}^d$ given by

$$s(t, x) := \nabla_x \log p_t(x).$$

Here and below, $p_t(x)$ denotes the density of $\mathcal{L}(x_t)$. To simulate the reverse-time SDE eq. (2), we replace the typically intractable score function by the so called *score network* $s_\theta : [0, \infty) \times \mathbb{R}^d \rightarrow \mathbb{R}^d$, a (deep) neural network which is trained to approximate the score function using the denoising score matching (DSM) objective

$$\mathbb{E}_{t \sim \mathcal{U}[0, T]} \left[\lambda(t) \mathbb{E}_{x_0, x_t} \|s_\theta(t, x_t) - \nabla \log p_{t|0}(x_t | x_0)\|^2 \right],$$

where $\nabla \log p_{t|0}(x_t | x_0)$ is the score of the conditional forward process $x_t | x_0$. Vincent et al. [27] showed that the DSM objective is equivalent to minimizing the expected squared error with respect to the true score:

$$\mathbb{E}_{t \sim \mathcal{U}[0, T]} \left[\lambda(t) \mathbb{E}_{x_t} \|s_\theta(t, x_t) - s(t, x_t)\|^2 \right].$$

With a score approximation at hand, we generate approximate samples from \mathcal{P}_0 by simulating the reverse-time SDE eq. (2) from an initial Gaussian distribution, since the true terminal law $\mathcal{L}(x_T)$ is generally unavailable. As a result, diffusion models inherit three central sources of error:

- (i) an *initialization error*, arising from starting the reverse process at a homogeneous Gaussian distribution $\mathcal{N}(0, \sigma^2 I_d)$ instead of $\mathcal{L}(x_T)$,
- (ii) a *score-matching error*, due to replacing the true score s with a neural network approximation s_θ , and
- (iii) a *discretization error*, introduced by the numerical scheme used to simulate the reverse-time SDE eq. (2).

In this work, we provide a numerical analysis for general discretization methods applied to the SDEs used in generative diffusion models. We complement the theoretical analysis with extensive simulations on both toy examples and standard image-generation benchmarks. Beyond clarifying the behavior of existing solvers, our results also lead to practical parameter-selection guidelines, helping to identify where computational resources are best invested when designing new diffusion models.

1.2 Related Works

Previous error bounds results for generative diffusion model discretizations that consider all three error sources have primarily been derived in TV or KL divergence, see [20, 2, 18]. More recently, several works have considered the 2-Wasserstein distance, which is known to correlate well with human perceptual similarity [22] and is related to the widely used Fréchet Inception Distance (FID) (cf. Subsection 3.2 for details). Similar to our analysis in Subsection 2.2, most of these contributions assume that the data distribution is strongly log-concave to bound the initialization error (i), including [6, 11, 26, 28, 8]. However, these works typically restrict attention to a smaller class of forward SDEs than us, analyze alternative discretization schemes, or only obtain the suboptimal $\mathcal{O}(\sqrt{h})$ convergence rate for Euler-Maruyama. Crucially, no contribution analyses the effect of using higher-order discretization schemes. Moreover, convergence is either studied only in small-scale numerical experiments or not investigated numerically at all. Because the assumption of strong log-concavity is quite restrictive, several works tried to relax or interchange this assumption. One line of research avoids strong log-concavity by assuming that p_0 has *bounded support*, as in [3, 19]. This assumption is not inherently more general, because neither bounded support nor strong log-concavity subsumes the other, and these works again focus on more restrictive forward processes, obtain weaker bounds, or analyze different numerical methods. One further work, [23], extends convergence guarantees beyond the log-concave setting, but only for Ornstein–Uhlenbeck-type SDEs and with initialization error rates that appear suboptimal in light of our empirical observations.

In addition to the choice of assumptions on the data distribution, another point of contention in the literature concerns the appropriate assumptions on the score-matching error. Most existing works, e.g. [11, 28, 26] assume that the error between the true score function and the learned score network is bounded when evaluated along the iterates of the EM scheme. However, as noted in [3], this assumption is somewhat unnatural, since it does not correspond to the actual training objective.

Overall, no current works analyze higher-order discretization schemes theoretically, and numerical experiments remain sparse. Furthermore, no existing work addresses a central open question in the field: why do higher-order solvers often fail to outperform Euler–Maruyama in practice? (cf. [15, 14] for empirical studies of this phenomenon.)

1.3 Our Contribution

Our first contribution is an all-at-once analysis, i.e. an analysis that considers all three error-sources of the EM scheme, see Theorem 2.5. Compared to existing results, our analysis especially covers a broader class of forward SDEs. Keeping the analysis sufficiently general is important, as it has been shown that choosing an optimal *noise schedule*, that is, an appropriate choice of the coefficient functions a and b , can significantly improve the performance of generative diffusion models [9]. Moreover, we derive an optimal parameter selection rule in Theorem 2.7 in respect to the step size of the discretization method, which is the dominant factor affecting generation time. To the best of our knowledge, this parameter choice rule is the first of its kind in GDM literature. Another advantage over previous works is that, as shown in Theorem 2.6, our analysis remains valid irrespective of the specific assumptions imposed on the score-matching error. Our second contribution is a general theorem that bounds the total error of any discretization method with a known strong L_2 convergence order p , see Theorem 2.9. Although this result requires assuming a bounded terminal time T , it has the key advantage of completely bypassing the need for assumptions on the data distribution, as it is formulated under the absence of initialization error. Using this theorem we improve upon Theorem 2.5 by showing an enhanced convergence rate regarding the discretization error of the EM method. Employing Theorem 2.9, we derive a higher order discretization method specifically tailored to the class of SDEs considered in this work. To the best of our knowledge, this is the first higher-order stochastic sampler with guaranteed convergence order in the setting of GDMs. Finally, we present extensive numerical experiments demonstrating that the predicted error bounds are observable in practice, both for toy problems where the data distribution is a Gaussian (mixture) and a real world benchmark dataset in CIFAR-10 [17]. Overall, the theoretical analysis and numerical experiments both provide further insight into the often observed empirical superiority of EM in comparison to higher-order solvers.

1.4 Notation and Problem Setup

Throughout this work, we study forward processes with spatially linear drift f and spatially independent diffusion coefficient g , i.e. processes of the form

$$dx_t = -f(t)x_t dt + g(t) dW_t, \quad x_0 \sim \mathcal{P}_0, \quad (3)$$

which include many diffusion models used in practice, cf. [25, 10, 11]. For processes of this type we can observe the following remark.

Remark 1.1. Conditioned on x_0 , the solution of the SDE eq. (3) can be derived explicitly as $x_t|x_0 \sim \mathcal{N}(\phi_f(t)x_0, \varphi_{f,g}(t))$, where

$$\phi_f(t) = e^{(-\int_0^t f(s) \, ds)} \quad \text{and} \quad \varphi_{f,g}(t) = \int_0^t e^{-2 \int_s^t f(v) \, dv} g^2(s) \, ds.$$

Assuming our coefficient functions are chosen such that $\lim_{t \rightarrow \infty} x_t \stackrel{D}{=} \mathcal{N}(0, I_d)$, and $f > 0$, we get $\lim_{t \rightarrow \infty} \phi_f(t) = 0$ and $\lim_{t \rightarrow \infty} \varphi_{f,g}(t) = 1$, as well as $0 \leq \phi_f(t) \leq 1$ and $0 \leq \varphi_{f,g}(t) \leq 1$ for $t \in [0, \infty)$. Moreover, $\phi_f(0) = 1$ and $\varphi_{f,g}(0) = 0$, and the functions $\phi_f(t)$ and $\varphi_{f,g}(t)$ are monotone, decreasing and increasing respectively.

Using the time-reversal formula eq. (2), the corresponding reverse-time dynamics are

$$dy_t = [f(\tau) y_t + g^2(\tau) s(\tau, y_t)] \, dt + g(\tau) \, dW_t, \quad y_0 \sim \mathcal{L}(x_T). \quad (4)$$

Furthermore, we consider the backward process to be initialized from $\mathcal{N}(0, \sigma_T^2 I_d)$, with $\sigma_T^2 := \varphi_{f,g}(T)$. We proceed by introducing the following processes:

$$dy_t^N = [f(\tau) y_t^N + g^2(\tau) s(\tau, y_t^N)] \, dt + g(\tau) \, dW_t, \quad y_0^N \sim \mathcal{N}(0, \sigma_T^2 I_d), \quad (5)$$

$$dy_t^\theta = [f(\tau) y_t^\theta + g^2(\tau) s_\theta(\tau, y_t^\theta)] \, dt + g(\tau) \, dW_t, \quad y_0^\theta \sim \mathcal{L}(x_T), \quad (6)$$

$$dy_t^{N,\theta} = [f(\tau) y_t^{N,\theta} + g^2(\tau) s_\theta(\tau, y_t^{N,\theta})] \, dt + g(\tau) \, dW_t, \quad y_0^{N,\theta} \sim \mathcal{N}(0, \sigma_T^2 I_d), \quad (7)$$

where we assume the driving Wiener process W_t is shared between eqs. (4) to (7). One can interpret y_t^N as being the process which introduces the initialization error, y_t^θ as being the process which introduces the score matching error, and $y_t^{N,\theta}$ as being the process which exhibits both error types. Furthermore, we denote the discretized version of any time continuous process x_t by \bar{x}_t . Thus, the process $\bar{y}_k^{N,\theta}$ exhibits all three error types. To simplify notation, we consider an equidistant discretization grid $0 = t_0 < t_1 < \dots < t_K = T$ with uniform step size $h = \frac{T}{K}$, and write $\tau_k = T - t_k$ for the reverse time discretization. However, we want to stress that all proofs also work on non equidistant discretizations. Finally, the constants $m, M, L \in \mathbb{R}$ will denote lower bounds, upper bounds, and Lipschitz constants with according indices.

2 Assumptions and Main Result

In this section, we present our two main results. The first concerns the convergence order of the Euler–Maruyama (EM) method and can be found in Theorem 2.5. Its proof is more technical than the one of the subsequent results, but it has the advantage of accounting for all three sources of error while relying on less restrictive assumptions. By assuming a fixed terminal time T and no initialization error, we can establish a more general convergence result in Theorem 2.9, which establishes error bounds for any discretization method with known L_2 convergence order.

2.1 Assumptions and Merit Discussion

To analyze the reverse-time SDE and its discretization, we impose several structural assumptions.

Assumption 1. (existence of solution) *We assume $\|x_0\|_{L_2} < \infty$ for $x_0 \sim \mathcal{P}_0$ and all SDEs eqs. (3) to (7) admit strong solutions.*

Assumption 2. (regularity of the data distribution) *We assume \mathcal{P}_0 has the density p_0 w.r.t. the d -dimensional Lebesgue measure, and that p_0 is twice differentiable and positive everywhere. Moreover, $-\log p_0$ is m_0 -strongly convex and L_0 -smooth for some $m_0, L_0 > 0$, i.e.*

$$m_0 I_d \preceq \nabla^2(-\log p_0(x)) \preceq L_0 I_d, \quad \text{for all } x,$$

where \preceq is the Loewner order for symmetric matrices.

Assumption 3. (score matching error bound)

3.A. *There exists some $\varepsilon > 0$ with*

$$\sup_{k=0,1,\dots,K} \left\| s\left(\tau_k, \bar{y}_k^{\mathcal{N},\theta}\right) - s_\theta\left(\tau_k, \bar{y}_k^{\mathcal{N},\theta}\right) \right\|_{L_2} \leq \varepsilon.$$

3.B. *There exists some $\varepsilon' > 0$ such that*

$$\sup_{\tau \in [0,T]} \left\| s(\tau, y_\tau) - s_\theta(\tau, y_\tau) \right\|_{L_2} \leq \varepsilon'.$$

Assumption 4. (regularity of the score function)

4.A. *We assume that the Fisher Information of the data distribution \mathcal{P}_0 is finite, i.e.*

$$\mathbb{E} [\|s(0, x_0)\|^2] < \infty.$$

Furthermore, we assume the score function to be Lipschitz in time, i.e. there exists a constant $L_{s,t} > 0$ with

$$\sup_{k=1,\dots,K} \sup_{\tau_k \leq \tau \leq \tau_{k-1}} \|s(\tau, x) - s(\tau_k, x)\| \leq L_{s,t} h (1 + \|x\|)$$

4.B. *In addition to Assumption 4.A, assume the score function to be Lipschitz in space with constant $L_{s,x}$.*

Assumption 5. (regularity of the score network)

5.A. *We assume the learned score network s_θ to be Lipschitz continuous and of linear growth.*

5.B. *The score network has bounded derivatives in time and space up to third order.*

5.C. *The score network has bounded derivatives in time and space up to fifth order.*

Assumption 6. (model parameters) *In general, we assume f and g are chosen such that $\lim_{t \rightarrow \infty} x_t \stackrel{D}{=} \mathcal{N}(0, I_d)$, f and g to be bounded, and $f > 0$.*

- 6.A. *We assume f and g in eq. (3) to be Lipschitz continuous and of linear growth.*
- 6.B. *We assume all derivatives of f and g are bounded up to third order.*
- 6.C. *We assume all derivatives of f and g are bounded up to fifth order.*

We proceed by discussing the practicality of the assumptions stated above.

Assumption 1 is a standard assumption in SDE discretization, and could be omitted partially. For example, Assumption 6.A and $\|x_0\|_{L_2} < \infty$ implies that the SDE eq. (3) admits a strong solution, which together with any Assumption 5.A to Assumption 5.C implies, that the SDEs eqs. (6) and (7) admit strong solutions as well. Furthermore, by adding the assumption of a linearly growing score function, all other SDEs also admit strong solutions under Assumptions 4.B and 6.A, cf. [5, Chapter II, § 7].

Assumption 2 is standard in much of the existing literature, see [6, 11, 26, 28, 8]. As mentioned in Subsection 1.2, recent works have attempted to weaken it. Some approaches, such as [3, 19], assume that the support of p_0 is bounded; however, this assumption is not strictly weaker than strong log concavity and excludes natural examples like a Gaussian data distribution. Other work, such as [23], successfully relaxes the assumption to p_0 being weakly log-concave with a Lipschitz gradient of the exponent.

We emphasize that Assumption 2 is only used in Subsection 2.2 and not for Theorem 2.9. Furthermore, in Section 3, we consider experiments with data distributions that are not strongly log-concave and show that our bounds still appear to hold in this setting.

Assumption 3.A is clearly proof-driven and represents the minimal condition required for the proof of Theorem 2.5 to work. In contrast, Assumption 3.B is the more natural assumption as discussed in [3], as it is directly bounded by the learning objective. We note that when additionally imposing Assumption 5.A, one can prove Theorem 2.5 under Assumption 3.B as well and retain all its conclusions, cf. Theorem 2.6.

Assumption 4.A imposes square integrability on the score only at $t = 0$, which is expanded by Theorem 2.2 to all $t \in [0, T]$. Moreover, Assumption 4.B is only used in Subsection 2.3 where we do not assume Assumption 2, because under Assumption 2 Lipschitz continuity is implied, see Theorem 2.1.

Assumption 5: Since we have full control over how we choose the score network, it is quite easy in practice to construct a network that fulfills all three assumptions in Assumption 5. Furthermore, we want to note the following implication Assumptions: 5.C \Rightarrow 5.B \Rightarrow 5.A.

Assumption 6: The conditions that f and g are chosen such that $\lim_{t \rightarrow \infty} x_t \stackrel{D}{=} \mathcal{N}(0, I_d)$ is a standard assumption in GDM literature. As mentioned before, the variance could also be different from 1 as long as its value is known. Assuming additionally that f and g are bounded, and that $f > 0$ allows for simplified proofs. Relaxing these conditions to more general settings is straightforward but results in longer, though not more difficult, proofs. However, those conditions are satisfied for all practical GDMs. The Lipschitz and linear growth conditions are common in SDE theory and ensure that the SDE eq. (3) admits a strong solution, cf. Assumption 1. Similar to Assumption 5, Assumptions 6.B and 6.C imply Assumption 6.A. We also want to note that in Subsection 2.3, the boundedness of f and g follow from their regularity and the bounded T assumption.

Remark 2.1. [11, Lemma 9] shows that Assumption 2 implies Assumption 4.B. Furthermore, combining Theorem 1.1 with [11, (3.6)], which provides the bound

$$L_{s,x}(t) = \min \left\{ \frac{1}{\varphi_{f,g}(t)}, \frac{L_0}{\phi_f^2(t)} \right\},$$

we obtain that the Lipschitz constant of the score function is uniformly bounded on $[0, \infty)$. In particular $\sup_{0 \leq t \leq T} L_{s,x}(t) \leq L_{s,x} < \infty$.

2.2 A Convergence Result for Euler–Maruyama

In this section, we conduct our analysis in the same spirit as [11]. Although we work under the same set of assumptions and draw on some of their arguments, most notably those in [11, Proposition 7, Lemma 9,10], our approach and conclusions differ in several essential aspects. The most significant difference is that we study asymptotic convergence, which is not addressed in their work. Recall that the EM discretization of a general SDE eq. (1) is given by the single update step

$$\bar{x}_{k+1} = \bar{x}_k + a(t_k, \bar{x}_k)h + b(t_k, \bar{x}_k)\Delta W_{t_k},$$

with $\Delta W_{t_k} = W_{t_{k+1}} - W_{t_k}$. Thus, the EM discretization of eq. (7) is given by

$$\bar{y}_{k+1}^{\mathcal{N},\theta} = \bar{y}_k^{\mathcal{N},\theta} + \left(f(\tau_k) \bar{y}_k^{\mathcal{N},\theta} + g^2(\tau_k) s_\theta(\tau_k, \bar{y}^{\mathcal{N},\theta}) \right) h + g(\tau_k) \Delta W_{t_k}. \quad (8)$$

With the EM scheme established, we proceed by showing that the finiteness of the Fisher Information of the score at $t = 0$ assumed in Assumption 4.A extends to any t .

Lemma 2.2. Under Assumptions 4.A and 6.A, the Fisher information of the reverse–time process satisfies

$$I(y_t) = \mathbb{E}[\|s(\tau, y_t)\|^2] \leq c_{Fisher}, \quad t \in [0, T],$$

for some constant $c_{Fisher} < \infty$.

Proof. Since y_t has the same law as the forward solution x_{T-t} , it suffices to bound the Fisher information of x_t . From Theorem 1.1 we get $x_t = V_t^1 + V_t^2$, with $V_t^1 = \phi_f(t)x_0$ and $V_t^2 \sim \mathcal{N}(0, \varphi_{f,g}(t)I_d)$ independent. The scaling property of the Fisher information yields $\mathcal{I}(V_t^1) = \frac{1}{\phi_f^2(t)}\mathcal{I}(x_0)$. For $V_t^2 \sim \mathcal{N}(0, \varphi_{f,g}(t)I_d)$ the Fisher information equals $\mathcal{I}(V_t^2) = \frac{d}{\varphi_{f,g}^2(t)}$. The Blachman-Stam Fisher information inequality [4] for independent summands yields

$$\mathcal{I}(x_t) \leq \frac{1}{\mathcal{I}(V_t^1)^{-1} + \mathcal{I}(V_t^2)^{-1}} = \left(\frac{\phi_f^2(t)}{\mathcal{I}(x_0)} + \frac{\varphi_{f,g}(t)}{d} \right)^{-1} = \frac{\mathcal{I}(x_0) d}{\phi_f^2(t)d + \varphi_{f,g}(t)\mathcal{I}(x_0)}.$$

The denominator consists of the strictly increasing $0 < \varphi_{f,g}(t)\mathcal{I}(x_0) < \mathcal{I}(x_0)$ and the strictly decreasing $0 < \phi_f^2(t)d < d$. Furthermore, both functions are continuous in respect to t , and hence $m = \min_{t \in \mathbb{R}_0^+} \{\phi_f^2(t)d + \varphi_{f,g}(t)\mathcal{I}(x_0)\} > 0$. This shows

$$\mathcal{I}(x_t) \leq \frac{\mathcal{I}(x_0)d}{m} =: c_{\text{Fisher}}$$

for all t . \square

Note that the Fisher information inequality from [4] employed above is stated there only for the one-dimensional case, but the proof can readily be adapted to work for the multi-dimensional case. Before stating the main theorem and its proof, we show two technical lemmas that bounds the error of the EM method in a single step and some constants used.

Lemma 2.3. *Under Assumptions 2,3.A,4.A and 6.A, the difference of the reverse-time SDE starting at the normal distribution and its EM discretization is bounded in L_2 by:*

$$\|y_{t_{k+1}}^{\mathcal{N}} - \bar{y}_{k+1}^{\mathcal{N},\theta}\|_{L_2} \leq (1 + \mathcal{O}(h)) \|y_{t_k}^{\mathcal{N}} - \bar{y}_k^{\mathcal{N},\theta}\|_{L_2} + \mathcal{O}(h\sqrt{h}) + \mathcal{O}(h\varepsilon)$$

Proof. We will make use of the following bounds derived in the literature:

$$\sup_{t_k \leq t \leq t_{k+1}} \|y_t^{\mathcal{N}} - y_{t_k}^{\mathcal{N}}\|_{L_2} \leq \eta_{k,h} \quad (\text{cf. [11, Lemma 10]}) \quad (9)$$

$$\sup_{t_k \leq t \leq t_{k+1}} \|y_t^{\mathcal{N}} - y_t\|_{L_2} \leq c_1(T) \quad (\text{cf. [11, (A.6)]}) \quad (10)$$

$$\sup_{t_k \leq t \leq t_{k+1}} \|y_t\|_{L_2} \leq c_2(T) \quad (\text{cf. [11, (5.14)]}) \quad (11)$$

Furthermore, we note that for a deterministic, integrable function f and a family of random variables or process x_t such that $\sup_{t_{k-1} \leq t \leq t_k} \|x_t\|_{L_2} < \infty$, we have

$$\left\| \int_k^{k+1} f(t) x_t dt \right\|_{L_2} \leq \sup_{t_k \leq t \leq t_{k+1}} \|x_t\|_{L_2} \left(h \int_k^{k+1} f^2(t) dt \right)^{\frac{1}{2}} < \infty \quad (12)$$

by using the convexity of the Euclidean norm, the Cauchy-Schwarz inequality and Fubini's theorem. To compare the continuous time reverse process $y_t^{\mathcal{N}}$ and the EM discretization $\bar{y}_k^{\mathcal{N},\theta}$, we represent both in integral form:

$$y_{t_{k+1}}^{\mathcal{N}} = y_{t_k}^{\mathcal{N}} + \int_k^{k+1} f(\tau) y_t^{\mathcal{N}} + g^2(\tau) s(\tau, y_t^{\mathcal{N}}) dt + \int_k^{k+1} g(\tau) dW_t \quad (13)$$

$$\bar{y}_{k+1}^{\mathcal{N},\theta} = \bar{y}_k^{\mathcal{N},\theta} + \int_k^{k+1} f(\tau_k) \bar{y}_k^{\mathcal{N},\theta} + g^2(\tau_k) s_\theta(\tau_k, \bar{y}_k^{\mathcal{N},\theta}) dt + \int_k^{k+1} g(\tau_k) dW_t. \quad (14)$$

By adding zeros to $y_{t_{k+1}}^{\mathcal{N}} - \bar{y}_{k+1}^{\mathcal{N},\theta}$ and expanding the norm we get

$$\begin{aligned} \|y_{t_{k+1}}^{\mathcal{N}} - \bar{y}_{k+1}^{\mathcal{N},\theta}\|_{L_2} &\leq \|y_{t_k}^{\mathcal{N}} - \bar{y}_k^{\mathcal{N},\theta}\|_{L_2} \\ &\quad + \left\| \int_k^{k+1} f(\tau_k) (y_{t_k}^{\mathcal{N}} - \bar{y}_k^{\mathcal{N},\theta}) + g^2(\tau_k) (s(\tau, y_t^{\mathcal{N}}) - s(\tau, \bar{y}_k^{\mathcal{N},\theta})) dt \right\|_{L_2} \\ &\quad + \left\| \int_k^{k+1} f(\tau_k) (y_t^{\mathcal{N}} - y_{\tau_k}^{\mathcal{N}}) + g^2(\tau_k) (s(\tau, y_t^{\mathcal{N}}) - s(\tau, y_{\tau_k}^{\mathcal{N}})) dt \right\|_{L_2} \\ &\quad + \left\| \int_k^{k+1} (f(\tau) - f(\tau_k)) y_t^{\mathcal{N}} + (g^2(\tau) - g^2(\tau_k)) s(\tau, y_t^{\mathcal{N}}) dt \right\|_{L_2} \\ &\quad + \left\| \int_k^{k+1} g^2(\tau_k) (s(\tau, \bar{y}_k^{\mathcal{N},\theta}) - s_\theta(\tau_k, \bar{y}_k^{\mathcal{N},\theta})) dt \right\|_{L_2} \\ &\quad + \left\| \int_k^{k+1} g(\tau) - g(\tau_k) dW_t \right\|_{L_2}. \end{aligned}$$

We proceed by bounding each term individually.

Bounding the first term: We have that

$$\begin{aligned} &\left\| \int_k^{k+1} f(\tau_k) (y_{t_k}^{\mathcal{N}} - \bar{y}_k^{\mathcal{N},\theta}) + g^2(\tau_k) (s(\tau, y_t^{\mathcal{N}}) - s(\tau, \bar{y}_k^{\mathcal{N},\theta})) dt \right\|_{L_2} \\ &= \left\| h f(\tau_k) (y_{t_k}^{\mathcal{N}} - \bar{y}_k^{\mathcal{N},\theta}) + h g^2(\tau_k) (s(\tau, y_t^{\mathcal{N}}) - s(\tau, \bar{y}_k^{\mathcal{N},\theta})) \right\|_{L_2} \\ &\leq h (f(\tau_k) + g^2(\tau_k) L_{s,x}) \left\| (y_{t_k}^{\mathcal{N}} - \bar{y}_k^{\mathcal{N},\theta}) \right\|_{L_2}. \end{aligned}$$

Bounding the second term: We use the bound for $\sup_{t_k \leq t \leq t_{k+1}} \|y_t^{\mathcal{N}} - y_{t_k}^{\mathcal{N}}\|_{L_2}$ in eq. (9) and eq. (12) to get:

$$\begin{aligned} &\left\| \int_k^{k+1} f(\tau_k) (y_t^{\mathcal{N}} - y_{\tau_k}^{\mathcal{N}}) + g^2(\tau_k) (s(\tau, y_t^{\mathcal{N}}) - s(\tau, y_{\tau_k}^{\mathcal{N}})) dt \right\|_{L_2} \\ &\leq h f(\tau_k) \sup_{t_k \leq t \leq t_{k+1}} \|y_t^{\mathcal{N}} - y_{t_k}^{\mathcal{N}}\|_{L_2} + h g^2(\tau_k) L_{s,x} \sup_{t_k \leq t \leq t_{k+1}} \|y_t^{\mathcal{N}} - y_{t_k}^{\mathcal{N}}\|_{L_2} \\ &= h (f(\tau_k) + g^2(\tau_k) L_{s,x}) \sup_{t_k \leq t \leq t_{k+1}} \|y_t^{\mathcal{N}} - y_{t_k}^{\mathcal{N}}\|_{L_2} \end{aligned}$$

Bounding the third term: We use the bounds for $\sup_{t_k \leq t \leq t_{k+1}} \|y_t^N - y_t\|_{L_2}$ from eq. (11), $\sup_{t_k \leq t \leq t_{k+1}} \|y_t\|_{L_2}$ from eq. (10), as well as the bound for $\sup_{t_k \leq t \leq t_{k+1}} \|s(\tau, y_t)\|_{L_2}$ from Theorem 2.2. First, we split the expression.

$$\left\| \int_k^{k+1} (f(\tau) - f(\tau_k)) y_t^N + (g^2(\tau) - g^2(\tau_k)) s(\tau, y_t^N) dt \right\|_{L_2}$$

once more and bound the parts individually. Bounding the first part:

$$\begin{aligned} & \left\| \int_k^{k+1} (f(\tau) - f(\tau_k)) y_t^N dt \right\|_{L_2} \\ &= \left\| \int_k^{k+1} (f(\tau) - f(\tau_k)) (y_t^N - y_t) dt + \int_k^{k+1} (f(\tau) - f(\tau_k)) y_t dt \right\|_{L_2} \\ &\leq \sqrt{h \int_k^{k+1} (f(\tau) - f(\tau_k))^2 dt} \left(\sup_{t_k \leq t \leq t_{k+1}} \|y_t^N - y_t\|_{L_2} + \sup_{t_k \leq t \leq t_{k+1}} \|y_t\|_{L_2} \right). \end{aligned}$$

To get the last inequality we use the triangle inequality of the norm and use eq. (12). Bounding the second part works analogously:

$$\begin{aligned} & \left\| \int_k^{k+1} (g^2(\tau) - g^2(\tau_k)) s(\tau, y_t^N) dt \right\|_{L_2} \\ &\leq L_{s,x} \sqrt{h \int_k^{k+1} (g^2(\tau) - g^2(\tau_k))^2 dt} \\ &\quad \cdot \left(\sup_{t_k \leq t \leq t_{k+1}} \|y_t^N - y_t\|_{L_2} + \sup_{t_k \leq t \leq t_{k+1}} \|s(\tau, y_t)\|_{L_2} \right). \end{aligned}$$

Bounding the fourth term: We add $0 = s(\tau_k, \bar{y}_k^{N,\theta}) - s(\tau_k, \bar{y}_k^{N,\theta})$ and use eq. (12) and Assumptions 3.A and 4.A to get

$$\begin{aligned} & \left\| \int_k^{k+1} g^2(\tau_k) (s(\tau, \bar{y}_k^{N,\theta}) - s(\tau_k, \bar{y}_k^{N,\theta})) dt \right\|_{L_2} \\ &\leq h g^2(\tau_k) \left(\varepsilon + L_{s,t} h \left(1 + \|\bar{y}_k^{N,\theta}\|_{L_2} \right) \right) \\ &\leq h g^2(\tau_k) \left(\varepsilon + L_{s,t} h \left(1 + \|\bar{y}_k^{N,\theta} - y_{t_k}^N\|_{L_2} + \|y_{t_k}^N - y_{t_k}\|_{L_2} + \|y_{t_k}\|_{L_2} \right) \right) \\ &\leq h g^2(\tau_k) \left(\varepsilon + L_{s,t} h \left(1 + \|\bar{y}_k^{N,\theta} - y_{t_k}^N\|_{L_2} + \|x_0\|_{L_2} + \|y_{t_k}\|_{L_2} \right) \right), \end{aligned}$$

where $\|y_{t_k}^N - y_{t_k}\|_{L_2} \leq \|x_0\|_{L_2}$ was shown in [11, (5.12)].

Bounding the last Term: Using the Ito-Isometry we get

$$\begin{aligned} \left\| \int_k^{k+1} g(\tau) - g(\tau_k) \, dW_t \right\|_{L_2} &= \sqrt{\mathbb{E} \left[\left\| \int_k^{k+1} g(\tau) - g(\tau_k) \, dW_t \right\|_2^2 \right]} \\ &= \sqrt{d \int_k^{k+1} (g(\tau) - g(\tau_k))^2 \, dt} \end{aligned}$$

With the bounds from eqs. (9) to (11), Theorem 2.1 and Theorem 2.2 we obtain

$$\begin{aligned} \|y_{t_{k+1}}^{\mathcal{N}} - \bar{y}_{k+1}^{\mathcal{N},\theta}\|_{L_2} &\leq (1 + h(f(\tau_k) + g^2(\tau_k) L_{s,x}) + h^2 g^2(\tau_k) L_{s,t}) \|y_{t_k}^{\mathcal{N}} - \bar{y}_k^{\mathcal{N},\theta}\|_{L_2} \\ &\quad + h(f(\tau_k) + g^2(\tau_k) L_{s,x}) \eta_{k,h} \\ &\quad + \sqrt{h \int_k^{k+1} (f(\tau) - f(\tau_k))^2 \, dt (c_1(T) + c_2(T))} \\ &\quad + L_{s,x} \sqrt{h \int_k^{k+1} (g^2(\tau) - g^2(\tau_k))^2 \, dt (c_1(T) + c_{\text{Fisher}})} \\ &\quad + hg^2(\tau_k) (\varepsilon + L_{s,t} h (1 + \|x_0\|_{L_2} + c_2(T))) \\ &\quad + \sqrt{d \int_k^{k+1} (g(\tau) - g(\tau_k))^2 \, dt} \end{aligned}$$

From Assumption 6.A it follows that

$$\begin{aligned} \sqrt{h \int_k^{k+1} (f(\tau) - f(\tau_k))^2 \, dt} &\leq \sqrt{L_f^2 h \int_k^{k+1} h^2 \, dt} \leq L_f h^2 \\ \sqrt{h \int_k^{k+1} (g^2(\tau) - g^2(\tau_k))^2 \, dt} &\leq \sqrt{h \int_k^{k+1} (L_g 2M_g h)^2 \, dt} \leq 2L_g M_g h^2 \\ \sqrt{d \int_k^{k+1} (g(\tau) - g(\tau_k))^2 \, dt} &\leq L_g h \sqrt{dh}. \end{aligned}$$

Using Theorem 2.4 and the boundedness of f and g , we get from inserting all bounds

$$\|y_{t_{k+1}}^{\mathcal{N}} - \bar{y}_{k+1}^{\mathcal{N},\theta}\|_{L_2} \leq (1 + \mathcal{O}(h)) \|y_{t_k}^{\mathcal{N}} - \bar{y}_k^{\mathcal{N},\theta}\|_{L_2} + \mathcal{O}(h\sqrt{h}) + \mathcal{O}(h\varepsilon)$$

□

The following lemma controls the asymptotic behavior of the three constants introduced in eqs. (9) to (11).

Lemma 2.4. *Under Assumption 6.A the constants from eqs. (9) to (11) satisfy*

$$c_1(T) = \mathcal{O}(1), \quad c_2(T) = \mathcal{O}(1) \quad \text{and} \quad \eta_{k,h} = \mathcal{O}(\sqrt{h})$$

Proof. From [11, (3.12)] we obtain

$$c_1(T) = \sup_{0 \leq t \leq T} \underbrace{\exp\left(-\frac{1}{2} \int_0^t m(T-s) \, ds\right) \phi_f(T)}_{=: \tilde{c}_1(t)} \|x_0\|_{L_2},$$

where $m(t) = \frac{2g^2(t)}{\frac{1}{m_0}\phi_f^2(t) + \varphi_{f,g}(t)} - 2f(t)$. By Theorem 1.1 we have $\frac{1}{m_0}\phi_f^2(t) \geq 0$, $\varphi_{f,g}(t) \geq 0$ and, similar to the proof of Theorem 2.2, $\min_{t \in \mathbb{R}_0^+} \{\frac{1}{m_0}\phi_f^2(t) + \varphi_{f,g}(t)\} > 0$, which implies

$$-2f(T-t) \leq m(T-t) \Rightarrow e^{\int_0^t f(T-s) \, ds} \geq e^{-\frac{1}{2} \int_0^t m(T-s) \, ds}.$$

Using this estimate in the expression for $\tilde{c}_1(t)$ yields

$$\tilde{c}_1(t) \leq \exp\left(\int_0^t f(T-s) \, ds\right) \phi_f(T) = \exp\left(-\int_0^{T-t} f(s) \, ds\right) \stackrel{f \geq 0}{\leq} 1,$$

and therefore $c_1(T) \leq \|x_0\|_{L_2} \in \mathcal{O}(1)$. Next, from [11, (3.13)] we have

$$c_2(T) = \sup_{0 \leq t \leq T} (\phi_f^2(t) \|x_0\|_{L_2} + d \varphi_{f,g}(t))^{1/2}.$$

Again using that f is nonnegative and Theorem 1.1, we obtain $\phi_f^2(t) \|x_0\|_{L_2} + d \varphi_{f,g}(t) \leq \|x_0\|_{L_2} + d$, and hence $c_2(T) \leq \|x_0\|_{L_2} + d \in \mathcal{O}(1)$. Finally, [11, Lemma 10] gives

$$\begin{aligned} \eta_{k,h} &= c_1(T) \int_k^{k+1} [f(T-s) + g^2(T-s) L_{s,x}] \, ds \\ &\quad + c_2(T) \int_k^{k+1} f(s) \, ds + \left(\int_{k-1}^k g^2(s) \, ds \right)^{1/2} \sqrt{d}. \end{aligned}$$

Since all integrands are bounded, this expression simplifies to

$$\eta_{k,h} = c_1(T) \mathcal{O}(h) + c_2(T) \mathcal{O}(h) + \mathcal{O}(\sqrt{h}) \sqrt{d}.$$

Combining this with the bounds on $c_1(T)$ and $c_2(T)$ shows that $\eta_{k,h} = \mathcal{O}(\sqrt{h})$. \square

With this lemma the preparations for the main theorem of this section are concluded.

Theorem 2.5. *Under Assumptions 1,2,3.A,4.A and 6.A we have that the 2-Wasserstein distance of the final iterate in the EM scheme $\bar{y}_K^{\mathcal{N},\theta}$ to the target distribution p_0 is of order*

$$\mathcal{W}_2\left(\mathcal{L}\left(\bar{y}_K^{\mathcal{N},\theta}\right), p_0\right) = \mathcal{O}\left(e^{-CT} + e^T \left[\sqrt{h} + \varepsilon\right]\right)$$

for $h, \varepsilon \rightarrow 0$ and $T \rightarrow \infty$ and a constant $C \geq 0$ explicitly stated in the proof below.

The proof proceeds by splitting the error into the continuous-time contraction error and the discretization error. The former follows from [11, Proposition 7]. The latter is controlled via the one-step estimate for the reverse SDE from Theorem 2.3.

Proof. First, we use the triangle inequality of the 2-Wasserstein distance:

$$\mathcal{W}_2 \left(\mathcal{L} \left(\bar{y}_K^{\mathcal{N}, \theta} \right), p_0 \right) \leq \mathcal{W}_2 \left(\mathcal{L} \left(y_T^{\mathcal{N}} \right), p_0 \right) + \mathcal{W}_2 \left(\mathcal{L} \left(\bar{y}_K^{\mathcal{N}, \theta} \right), \mathcal{L} \left(y_T^{\mathcal{N}} \right) \right)$$

Bounding $\mathcal{W}_2 \left(\mathcal{L} \left(y_T^{\mathcal{N}} \right), p_0 \right)$: With Assumption 2 we can use the result from [11, Lemma 7] to get

$$\mathcal{W}_2 \left(\mathcal{L} \left(y_T^{\mathcal{N}} \right), p_0 \right) \leq \exp \left(- \int_0^T c(t) dt \right) \|x_0\|_{L_2}$$

where $c(t) = \frac{m_0 g^2(t)}{D_1 + D_2}$, $D_1 = \phi_f^2(t)$ and $D_2 = m_0 \varphi_{f,g}(t)$. From Theorem 1.1 we get that $D_1 \leq 1$ and $D_2 \leq m_0$. Using the (lower) boundedness of g , we get

$$c(t) \geq \frac{m_0 m_g^2}{1+m_0} =: C \quad (15)$$

Using this bound and $\|x_0\|_{L_2} < \infty$ from Assumption 1 we get

$$\mathcal{W}_2 \left(\mathcal{L} \left(y_T^{\mathcal{N}} \right), p_0 \right) \leq \exp(-TC) \|x_0\|_{L_2} = \mathcal{O}(\exp(-CT))$$

Bounding $\mathcal{W}_2 \left(\mathcal{L} \left(\bar{y}_K^{\mathcal{N}, \theta} \right), \mathcal{L} \left(y_T^{\mathcal{N}} \right) \right)$: Suppose we define the error at step k as $e_k := \|y_{t_k}^{\mathcal{N}} - \bar{y}_k^{\mathcal{N}, \theta}\|_{L_2}$ and note that due to Theorem 2.3 we have

$$e_k \leq (1 + \mathcal{O}(h)) e_{k-1} + \epsilon(h, \varepsilon),$$

where $\epsilon(h, \varepsilon) = \mathcal{O}(h\sqrt{h}) + \mathcal{O}(h\varepsilon)$, and the initial condition is $e_0 = 0$. We apply a discrete Grönwalls argument and unroll the recurrence iteratively:

$$e_K \leq \epsilon(h, \varepsilon) \sum_{j=0}^{K-1} (1 + \mathcal{O}(h))^j = \epsilon(h, \varepsilon) \frac{(1+\mathcal{O}(h))^K - 1}{\mathcal{O}(h)}.$$

To estimate the geometric factor, note that $K = T/h$, which yields $(1 + \mathcal{O}(h))^{T/h} = e^{\mathcal{O}(T)} = \mathcal{O}(e^T)$ as $h \rightarrow 0$. Substituting this and the definition of $\epsilon(h, \varepsilon)$ into the previous inequality yields

$$e_K = \mathcal{O}(e^T) \left[\mathcal{O}(\sqrt{h}) + \mathcal{O}(\varepsilon) \right],$$

which, together with the first part, completes the proof. □

The following remark shows that we obtain a similar result under Assumption 3.B instead of Assumption 3.A when additionally assuming Assumption 5.A.

Remark 2.6. Adding Assumption 5.A to the Assumptions used in Theorem 2.5, we can decompose the score matching error to

$$\begin{aligned} \|s(\tau_k, \bar{y}_k^{\mathcal{N}, \theta}) - s_\theta(\tau_k, \bar{y}_k^{\mathcal{N}, \theta})\|_{L_2} &\leq (L_{s,x} + L_{s_\theta}) \left(\|y_k^{\mathcal{N}} - \bar{y}_k^{\mathcal{N}, \theta}\|_{L_2} + \|y_k^{\mathcal{N}} - y_k\|_{L_2} \right) \\ &\quad + \|s(\tau_k, y_k) - s_\theta(\tau_k, y_k)\|_{L_2}. \end{aligned}$$

From [11, Proof of Prop 8] and Assumption 6.A we get $\|y_k^{\mathcal{N}} - y_k\|_{L_2} \leq C_1 e^{-C_{\exp} T}$ for constants $C_1, C_{\exp} > 0$. This means that Assumption 3.B implies Assumption 3.A with

$$\varepsilon \leq \varepsilon' + (L_{s,x} + L_{s_\theta}) \left(\|y_k^{\mathcal{N}} - \bar{y}_k^{\mathcal{N}, \theta}\|_{L_2} \right) + C e^{-C_{\exp} T}$$

for some constant $C > 0$.

Furthermore, Theorem 2.5 allows us to choose the variable parameters h, ε and T in dependence of each other. We show this exemplary for ε and T in dependence of h , but in practice one could analogously choose h and T in dependence of ε , the latter being determined by the amount of computation during training.

Corollary 2.7. Using the constant $C > 0$ from Theorem 2.5 specified in eq. (15), one should choose the terminal time T and the training procedure (i.e. ε) such that

$$\varepsilon \sim \sqrt{h} \quad \text{and} \quad T \sim -\frac{1}{C+1} \log(\sqrt{h})$$

to achieve the optimal bound

$$\mathcal{W}_2 \left(\mathcal{L} \left(\bar{y}_K^{\mathcal{N}, \theta} \right), p_0 \right) = \mathcal{O} \left(h^{\frac{C}{2(C+1)}} \right).$$

2.3 A General Convergence Result

In this section, we will work with a fixed terminal time T . This allows us to analyze more general numerical schemes, as we can employ the so-called Ito–Taylor expansion (see [16, Chapter 5]) and leverage established convergence results that rely on it. Note that this results in a constant, non-vanishing initialization error, which is why we neglect its contribution in this section. The theorem we show in this section works for any discretization method for which the order p of strong L_2 convergence is known, i.e. a method for which

$$\sup_{0 \leq k \leq K} \|x_{t_k} - \bar{x}_k\|_{L_2} \leq C h^p, \tag{16}$$

holds for some constant C depending on the drift, the diffusion coefficient and the terminal time T only. To achieve these convergence results, it might be necessary to impose stronger differentiability conditions on the score network s_θ , cf. Assumptions 5.B and 5.C. We proceed by showing a lemma which allows us to bound the L_2 error introduced by the score network.

Lemma 2.8. *Under Assumptions 1, 3.B, 4.B, 5.A and 6.A and finite terminal time T we have*

$$\|y_T^\theta - y_T\|_{L_2} \leq C\varepsilon',$$

with some constant $C > 0$.

Proof. Set $\Delta(\tau) := y_T^\theta - y_T$ and $\Phi(u) = \|u\|_{L_2}$. We have

$$\Delta(T) = \Delta(0) + \int_0^T f(\tau) \Delta(\tau) d\tau + \int_0^T g^2(\tau) \left(s_\theta(\tau, y_\tau^\theta) - s(\tau, y_\tau) \right) d\tau.$$

Now, using $\Phi(\Delta(0)) = 0$ and taking the L_2 norm yields

$$\Phi(\Delta(T)) \leq \int_0^T \underbrace{\left(M_f + M_g^2 L_{s_\theta} \right)}_{=:B} \Phi(\Delta(\tau)) d\tau + \int_0^T g^2(\tau) \|s_\theta(\tau, y_\tau) - s(\tau, y_\tau)\|_{L_2} d\tau,$$

where we used Assumptions 1 and 5.A and Theorem 2.2, which follows from Assumptions 6.A and 4.B. Using Assumption 3.B and the integral Grönwall inequality, we get

$$\Phi(\Delta(T)) \leq \frac{e^{BT} - 1}{B} TM_g^2 \varepsilon' \leq C\varepsilon'$$

□

With this lemma the proof of the following theorem is straight-forward.

Theorem 2.9. *Let $\bar{y}_0^\theta, \dots, \bar{y}_K^\theta$ be the result of a discretization scheme of strong L_2 order p (cf. eq. (16)) applied to eq. (6). Grant Assumptions 1, 3.B, 4.B, 5.A and 6.A, as well as $T < \infty$ fixed. Then we get the error bound $\mathcal{W}_2(\mathcal{L}(\bar{y}_K^\theta), p_0) = \mathcal{O}(h^p + \varepsilon')$.*

Proof. We decompose the Wasserstein distance to

$$\mathcal{W}_2(\mathcal{L}(\bar{y}_K^\theta), \mathcal{L}(y_T)) \leq \mathcal{W}_2(\mathcal{L}(\bar{y}_K^\theta), \mathcal{L}(y_T^\theta)) + \mathcal{W}_2(\mathcal{L}(y_T^\theta), \mathcal{L}(y_T)).$$

We can control the first term by strong convergence results of discretization scheme with $\mathcal{W}_2(\mathcal{L}(\bar{y}_K^\theta), \mathcal{L}(y_T)) \leq \|\bar{y}_K^\theta - y_T^\theta\|_{L_2} = \mathcal{O}(h^p)$. The second term is bound using Theorem 2.8, which completes the proof. □

We can use this general theorem to formulate a corollary which improves the convergence in respect to the discretization error of the EM method from \sqrt{h} to h compared to Theorem 2.5.

Corollary 2.10. *Let $T > 0$ be fixed and consider eq. (6). Under Assumptions 1, 3.B, 4.B, 5.B and 6.B, as well as bounded T , we get the improved error bound*

$$\mathcal{W}_2(\mathcal{L}(\bar{y}_K^\theta), p_0) = \mathcal{O}(h + \varepsilon').$$

Underlying this corollary is the fact that the strong L_2 convergence order of the EM method is $p = 1$ in our setting, that is if the diffusion coefficient is spatially independent and, together with the drift, has bounded derivatives up to third order, cf. [16, Theorem 10.6.3 or Chapter 10.3]. Additionally to the EM method, we consider the following scheme introduced in [7] and extended to non-constant additive diffusion in [16, Chapter 11.3]. We discretize the general SDE eq. (1), but we assume the drift b to be spatially independent, i.e. $b(t, x_t) = b(t)$.

$$Q_k(x_k) = x_k + \frac{1}{2}ha(t_k, x_k) \quad (17a)$$

$$Q_k^*(x_k) = x_k + \frac{1}{2}ha(t_k, x_k) + \frac{3}{2}b(t_k)\sqrt{h}\beta \quad (17b)$$

$$P_k = b(t_k)\Delta W_n + (b(t_{k+1}) - b(t_k)) \left(\Delta W_{t_{k+1}} - \sqrt{h}\beta \right) \quad (17c)$$

$$x_{k+1} = x_k + \frac{1}{3}h \left[a \left(t_k + \frac{1}{2}h, Q_k(x_k) \right) + 2a \left(t_k + \frac{1}{2}h, Q_k^*(x_k) \right) \right] + P_k, \quad (17d)$$

where we define $\Delta W_{t_{k+1}} = W_{t_{k+1}} - W_{t_k}$ and $\beta = h^{-3/2} \int_{t_n}^{t_{n+1}} \Delta W_s \, ds$. How to simulate β in practice is described in [7, Chapter 7]. The following corollary is again a direct consequence of Theorem 2.9.

Corollary 2.11. *Under Assumptions 1, 3.B, 4.B, 5.C and 6.C, the method defined in eq. (17) has order of convergence*

$$\mathcal{W}_2 \left(\mathcal{L} \left(\bar{y}_K^{\mathcal{N}, \theta} \right), p_0 \right) = \mathcal{O} \left(h^{3/2} + \varepsilon' \right).$$

Again, this corollary relies on the 3/2-order L_2 convergence of the scheme eq. (17) under spatially independent drift and bounded derivatives of drift and diffusion up to 5th order, cf. [16, Theorem 11.5.2].

3 Experimental Results

In this section, we will compare the practical performance of the discussed discretizations in numerical examples.

3.1 Considered Problems

We consider four distributions as examples:

Problem 1. \mathcal{P}_0 is a 3072-dimensional Gaussian Mixture with four equally weighted components.

Problem 2. \mathcal{P}_0 is a 3072-dimensional Gaussian distribution.

Problem 3. \mathcal{P}_0 is the distribution of the CIFAR-10 dataset [17].

Problem 4. \mathcal{P}_0 is the distribution of the CIFAR-10 dataset in a latent space.

We choose the dimensionality of Problems 1 and 2 to match that of Problem 3 to stay close to real world applications. However, unlike for Problems 3 and 4, the score function for Problems 1 and 2 can be computed in closed form: Let $\mathcal{P}_0 = \sum_{k=1}^m \xi_k \mathcal{N}(\mu_k, \Sigma_k)$ be a Gaussian mixture with a probability vector $\xi \in [0, 1]^m$, and define $\Sigma_{k,t} = \phi(t)^2 \Sigma_k + \varphi(t) I$, and $\pi_{k,t}$ as the density of $\mathcal{N}(\phi(t) \mu_k, \Sigma_{k,t})$. Then, we have $p_t(x) = \sum_{k=1}^m \xi_k \pi_{k,t}(x)$, and the score function is

$$s(t, x) = \nabla \log p_t(x) = - \sum_{k=1}^m w_k(x) \Sigma_{k,t}^{-1} (x - \phi(t) \mu_k), \quad (18)$$

with weights $w_k(x) = \frac{\xi_k \pi_{k,t}(x)}{p_t(x)}$. Note that this score function fulfills Assumption 4.B. This closed-form representation allows for simulations without introducing a score-matching error and simulations where we can measure the exact score matching error ε from Assumption 3.A. Furthermore, while Problem 2 satisfies the strong log-concavity assumption, Problem 1 does not, which enables us to investigate the influence of this assumption. On the other hand, Problem 3 serves as a classical real-world benchmark in image generation [17]. Problem 4 is meant to illustrate the effect of different discretization schemes in the context of more modern GDMs, such as Stable Diffusion [21], which operate in a latent space. As encoder, we use the 2048-dimensional latent representations obtained from the penultimate layer of the Inception v3 model provided by the `pytorch_fid` repository. We emphasize that this experiment serves as a proof of concept: we do not generate images, only features in a latent space, since no public decoder exists. In all problems, we consider the forward SDE

$$dx_t = -\frac{1}{2}tx_t dt + \sqrt{t} dW_t, \quad \text{i.e.} \quad f(t) = -\frac{1}{2}t \quad \text{and} \quad g(t) = \sqrt{t},$$

which is the standard VP-SDE introduced in [25]. The parameter functions for this SDE fulfill all of Assumption 6 for bounded T . Furthermore, unless stated otherwise, we choose $T = 4$ as the terminal time. The score network is trained following the procedure described in [25], employing the *ddpm++* network architecture introduced therein. We choose this architecture to stay close to how GDMs are used in the real world, even though it is unclear if this network fulfills any of Assumption 5. To ensure comparability, we use the same model architecture and training procedure across all experiments, even though the *ddpm++* architecture, a U-Net-like convolutional neural network, is specifically designed for images in pixel space, i.e., for Problem 3. As a result, performance on the other considered problems could likely be improved by employing network architectures tailored to their respective data distributions.

3.2 Measuring the 2-Wasserstein Distance

To quantify the 2-Wasserstein distance between generated samples and the data distribution, we adopt a strategy similar to the widely used Fréchet Inception Distance (FID) [13]: We approximate both the data distribution \mathcal{P}_0 and the generated samples by Gaussians $\mathcal{N}(\mu_d, \Sigma_d)$ and $\mathcal{N}(\mu_g, \Sigma_g)$, where μ_d and Σ_d are the empirical mean and covariance of the

data, and μ_g and Σ_g are the empirical mean and covariance of our generated samples, respectively, and compute

$$\mathcal{W}_2 \left(\mathcal{P}_0, \mathcal{L} \left(\bar{y}_K^{\mathcal{N}, \theta} \right) \right) \approx \mathcal{W}_2 \left(\mathcal{N}(\mu_d, \Sigma_d), \mathcal{N}(\mu_g, \Sigma_g) \right).$$

However, unlike FID, which approximates the Gaussians in the Inception v3 latent space used for Problem 4, we compute the mean and variance directly in pixel space. A further difference to FID is our treatment of the covariance matrix: while FID employs the full covariance matrix, we often use a diagonal approximation. This choice is motivated by a practical issue from which FID also suffers, namely instability when only a small number of samples is available. This instability is more pronounced when using the full covariance matrix and further exacerbated as the dimensionality increases. As a result, using the full covariance matrix becomes ill-suited for measuring small \mathcal{W}_2 distances in high dimensions. This effect is clearly illustrated in table 1.

# of samples	10^5	$5 \cdot 10^5$	10^6	$5 \cdot 10^6$
\mathcal{W}_2 using diagonal Σ_g	0.679	0.302	0.215	0.096
\mathcal{W}_2 using full Σ_g	15.694	6.901	4.871	2.161

Table 1: Our \mathcal{W}_2 measure evaluated for different numbers of `torch.randn` samples and $\mathcal{N}(0, I_{3072})$.

In this experiment, we sample from a 3072-dimensional standard Gaussian using the `torch.randn` function and evaluate our \mathcal{W}_2 measure. Although the full covariance matrix offers better approximation properties in principle, these results motivate the use of a diagonal approximation for high dimensional problems. Accordingly, we use a diagonal covariance matrix for the high-dimensional settings in Problems 1 to 3. In contrast, for the relatively low-dimensional setting in Problem 4, we employ the full covariance matrix in order to retain its superior approximation properties. Finally, whenever the true mean and covariance of the data distribution are known, we use these quantities directly in our measure rather than relying on empirical approximations of μ_d and Σ_d . This applies to the toy problems in Problems 1 and 2 as well as to the experiment reported in table 1.

3.3 Evaluating Toy Problems

In fig. 1, we consider simulations using the true score function s and plot the step size h against $\mathcal{W}_2(h)$ and the terminal time T against $\mathcal{W}_2(T)$. We consider Problem 1 in the top row and Problem 2 on the bottom row. Each row consist of the EM method on the left and middle plot, and our higher order method eq. (17) on the right. Note that we have access to the true mean and variance of the data in both problems, which means we do not have to use the empirical mean and variance for our \mathcal{W}_2 evaluation. Since we use the true score function in generation, we discretize $y_t^{\mathcal{N}}$, and we choose the constant step size $h = \frac{4}{100}$ for the investigation of the terminal time T to keep the discretization error constant in this experiment. We simulate 300.000 samples for each sampler with each stepsize. The green regions along the x and y axes in the step sizes graphs indicate

stability: for large stepsizes, numerical methods for SDEs can become unstable even for simple test functions [16, Chapter 9.8], while for small \mathcal{W}_2 values, instability arises from the limited number of samples affecting our \mathcal{W}_2 estimation. Additionally, we plot reference functions for comparison and display the empirical convergence exponent ω_{LS} within the stability region, computed via least squares, i.e.

$$\begin{pmatrix} b_{LS} \\ \omega_{LS} \end{pmatrix} = \begin{pmatrix} 1 & \log(h_1) \\ \vdots & \vdots \\ 1 & \log(h_n) \end{pmatrix}^\dagger \begin{pmatrix} \log(\mathcal{W}_2(h_1)) \\ \vdots \\ \log(\mathcal{W}_2(h_n)) \end{pmatrix},$$

with A^\dagger being the Moore-Penrose inverse of a Matrix $A \in \mathbb{R}^{m \times n}$, $m, n \in \mathbb{N}$.

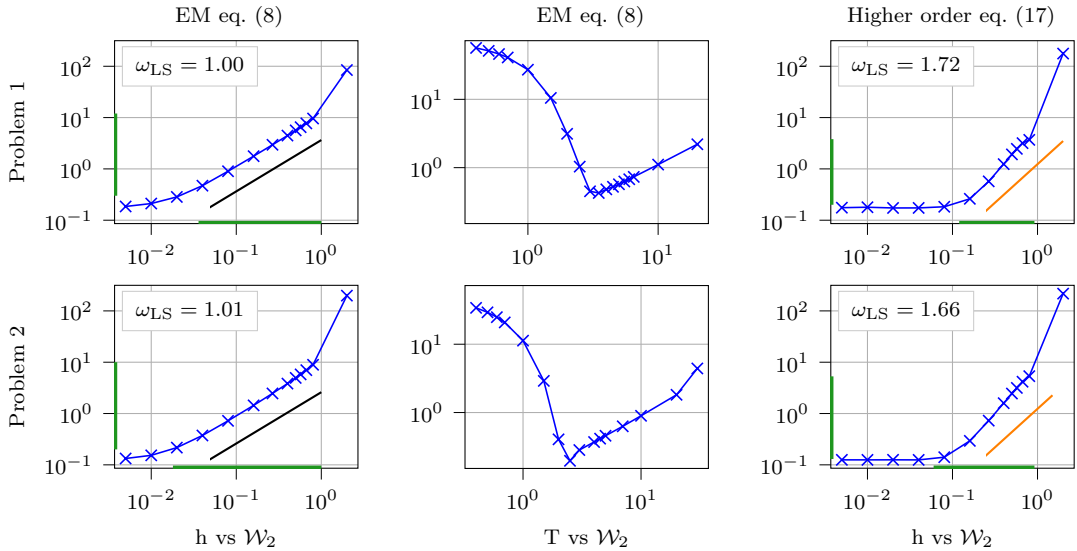


Figure 1: Simulations for Problems 1 and 2 using the true score function s , cf. eq. (18). The top row considers Problem 1, while the bottom row considers Problem 2. \mathcal{W}_2 of the EM method versus stepsize h on the left, \mathcal{W}_2 of the EM method versus the terminal time T in the middle, and \mathcal{W}_2 of the higher order method versus stepsize h on the right. Depicted is the empirical curve ($\text{---} \times \text{---}$), a reference line $\mathcal{O}(h)$ (---), and a reference line $\mathcal{O}(h^{3/2})$ (---). The green regions on the axes denote the stability region limited by the stepsize on the x-axis, and our \mathcal{W}_2 measure on the y-axis.

In fig. 2, we run simulations using a score network trained for 100 Epochs, that is, we discretize $y_t^{\mathcal{N}, \theta}$. Because of the computationally high cost of simulating using the score model, we reduce the number of samples generated to 50.000. Similar to fig. 1, the top row depicts Problem 1, while the bottom row depicts Problem 2. Each row shows three plots: on the left, the step size h versus the $\mathcal{W}_2(h)$ distance for the EM method, in the middle, the score-matching error ε versus the $\mathcal{W}_2(\varepsilon)$ distance for the EM method, and on the right, the step size h versus the $\mathcal{W}_2(h)$ distance for the considered higher-order

method. During EM-based generation, we evaluate the true score-matching error at each step using the true score function eq. (18), compute the empirical mean of the squared distances across steps, take the square root, and finally take the supremum to obtain ε . To keep the discretization error fixed, we use a constant step size $h = \frac{4}{100}$.

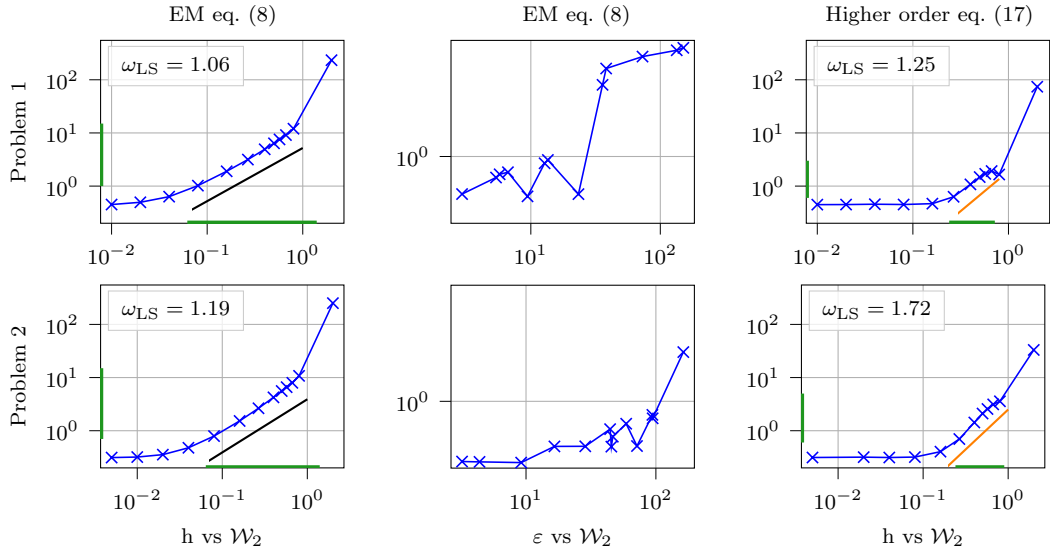


Figure 2: Simulations for Problems 1 and 2 using a learned score network s_θ which was trained for 100 Epochs. The top row considers Problem 1, while the bottom row considers Problem 2. \mathcal{W}_2 of the EM method versus stepsize h on the left, \mathcal{W}_2 of the EM method versus the score matching error ε in the middle, and \mathcal{W}_2 of the higher order method versus stepsize h on the right. Depicted is the empirical curve ($\text{---} \times \text{---}$), a reference line $\mathcal{O}(h)$ (---), and a reference line $\mathcal{O}(h^{3/2})$ ($\text{---} \textcolor{orange}{\times} \text{---}$). The green regions on the axes denote the stability region limited by the stepsize on the x-axis, and our \mathcal{W}_2 measure on the y-axis.

figs. 1 and 2 indicate that the convergence bounds established in Theorem 2.10 and Theorem 2.11 are consistent with empirical observations. Additionally, in the middle plot of fig. 1, we observe that \mathcal{W}_2 initially decays exponentially as T increases, but eventually grows exponentially for larger T . This behavior is consistent with the predictions of Theorem 2.5: for small T , the error is dominated by an exponentially decaying initialization error, while for large T , an exponentially growing discretization error becomes dominant. We can observe the same behavior even for Problem 1, which does not satisfy the log-concavity Assumption 2. The results concerning the score matching error ε shown in fig. 2 exhibit somewhat irregular behavior. This behavior can likely be attributed to two factors. First, the number of generated samples is relatively small, which limits our \mathcal{W}_2 evaluation function. Second, as shown in table 2, the best \mathcal{W}_2 value obtained from samples generated using the trained score model is already close to the optimal \mathcal{W}_2 value achievable at this stepsize, which corresponds to sampling without score-matching error, i.e., when sampling with the true score function. Consequently, small fluctuations inherent to the stochastic

sampling process can have a pronounced impact on the results.

	Problem 1	Problem 2
\mathcal{W}_2 using s	0.47083191	0.373251728
\mathcal{W}_2 using s_θ	0.61540787	0.47410081

Table 2: Comparison of \mathcal{W}_2 values using s and s_θ trained for 100 epochs.

3.4 Evaluating CIFAR-10

In fig. 3, we evaluate Problem 3 and Problem 4 using the EM method and our higher-order scheme eq. (17). The left panel reports performance for Problem 3 in terms of the \mathcal{W}_2 distance, while the middle panel shows the FID values for Problem 3. The right panel presents the \mathcal{W}_2 performance of the analyzed discretization methods for Problem 4. In this setup, samples are generated directly in the 2048-dimensional latent space in which the FID is computed and are evaluated using our \mathcal{W}_2 measure, effectively recovering the FID values. Again, we used the *ddmp++* network architecture and train it for 1000 epochs.

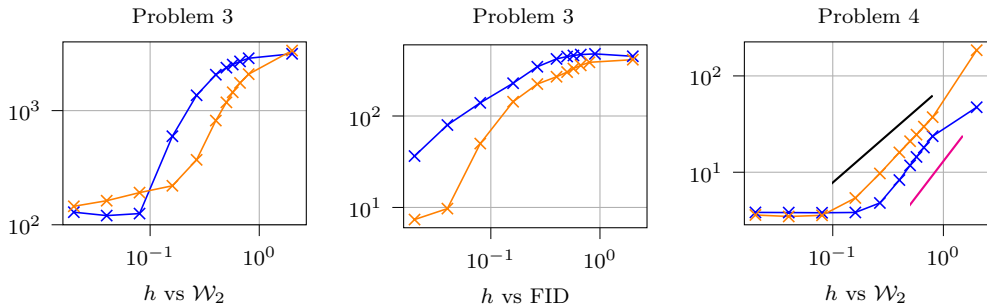


Figure 3: Simulations for Problem 3 and Problem 4. We show the empirical performance of the EM method (orange \times), the empirical performance of our higher order method eq. (17) (blue \times) and reference lines $\mathcal{O}(h)$ (black —) and $\mathcal{O}(h^{3/2})$ (magenta —).

fig. 3 demonstrates that the higher-order method seems to retain its faster convergence for Problem 3, even though the advantage is not as pronounced. The higher-order method still achieves lower absolute \mathcal{W}_2 distances for smaller step sizes, even though the EM method outperforms it for certain step sizes. In particular, the higher order method achieves $\mathcal{W}_2 = 125.37$ for $h = \frac{2}{25}$ which is not achieved by EM for any of our tested step sizes. However, this advantage disappears entirely when performance is measured using the FID score. This observation is not unexpected, as the relationship between distances in pixel space and those in latent space is not well understood and our predictions for Problem 3 would only hold in pixel space. However, looking at Problem 4, the advantage of using a higher order scheme is clearly visible. Although the EM method exhibits a better-than-expected convergence order, our higher-order method still achieves a steeper convergence slope. Compared to Problem 3, the advantage of the higher order method is

more pronounced in Problem 4, likely because the latent distribution is more regular than the pixel-space distribution, leading to a smoother score function that our network can approximate more accurately.

4 Conclusion

We presented a comprehensive analysis of the Euler–Maruyama scheme alongside a general result for the convergence of discretization methods in the diffusion model setting. Moreover, we presented a parameter choice rule that can help to identify where computational resources are best invested when designing new diffusion models. Furthermore, our theoretical findings were confirmed through a series of numerical experiments on both toy and real-world problems. Contrary to prior work, we showed that higher order methods can retain their theoretical advantage in terms of \mathcal{W}_2 in the GDM setting, even on real-world problems, and especially in latent space.

References

- [1] B. D. Anderson. Reverse-time diffusion equation models. *Stochastic Processes and their Applications*, 12(3):313–326, 1982.
- [2] J. Benton, V. De Bortoli, A. Doucet, and G. Deligiannidis. Nearly d -linear convergence bounds for diffusion models via stochastic localization. *ICLR*, 2024.
- [3] E. Beyler and F. Bach. Convergence of deterministic and stochastic diffusion-model samplers: A simple analysis in Wasserstein distance. *arXiv:2508.03210*, 2025.
- [4] N. Blachman. The convolution inequality for entropy powers. *IEEE Transactions on Information theory*, 11(2):267–271, 2003.
- [5] A. N. Borodin. *Stochastic processes*. Springer, 2017.
- [6] S. Bruno, Y. Zhang, D.-Y. Lim, Ömer Deniz Akyildiz, and S. Sabanis. On diffusion-based generative models and their error bounds: The log-concave case with full convergence estimates. *TMLR*, 2025.
- [7] C. C. Chang. Numerical solution of stochastic differential equations with constant diffusion coefficients. *Mathematics of computation*, 49(180):523–542, 1987.
- [8] S. Chen, S. Chewi, J. Li, Y. Li, A. Salim, and A. Zhang. Sampling is as easy as learning the score: theory for diffusion models with minimal data assumptions. In *NeurIPS, Workshop on Score-Based Methods*, 2022.
- [9] T. Chen. On the importance of noise scheduling for diffusion models. *arXiv:2301.10972*, 2023.

- [10] T. Dockhorn, A. Vahdat, and K. Kreis. Score-based generative modeling with critically-damped Langevin diffusion. *ICLR*, 2022.
- [11] X. Gao, H. M. Nguyen, and L. Zhu. Wasserstein convergence guarantees for a general class of score-based generative models. *Journal of machine learning research*, 26(43):1–54, 2025.
- [12] U. G. Haussmann and E. Pardoux. Time reversal of diffusions. *The Annals of Probability*, pages 1188–1205, 1986.
- [13] M. Heusel, H. Ramsauer, T. Unterthiner, B. Nessler, and S. Hochreiter. GANs trained by a two time-scale update rule converge to a local Nash equilibrium. In *NeurIPS*, volume 30, pages 6626–6637, 2017.
- [14] A. Jolicoeur-Martineau, K. Li, R. Piché-Taillefer, T. Kachman, and I. Mitliagkas. Gotta go fast with score-based generative models. *DLDE*, 2021.
- [15] T. Karras, M. Aittala, T. Aila, and S. Laine. Elucidating the design space of diffusion-based generative models. In *NeurIPS*, volume 35, pages 26565–26577, 2022.
- [16] P. Kloeden and E. Platen. *Numerical Solution of Stochastic Differential Equations*. Stochastic Modelling and Applied Probability. Springer Berlin Heidelberg, 2010.
- [17] A. Krizhevsky, V. Nair, and G. Hinton. Cifar-10 and cifar-100 datasets. <https://www.cs.toronto.edu/~kriz/cifar.html>, 2009.
- [18] H. Lee, J. Lu, and Y. Tan. Convergence for score-based generative modeling with polynomial complexity. In *NeurIPS*, volume 35, pages 22870–22882, 2022.
- [19] H. Lee, J. Lu, and Y. Tan. Convergence of score-based generative modeling for general data distributions. In *International Conference on Algorithmic Learning Theory*, pages 946–985, 2023.
- [20] G. Li, Y. Wei, Y. Chen, and Y. Chi. Towards faster non-asymptotic convergence for diffusion-based generative models. *ICLR*, 2024.
- [21] R. Rombach, A. Blattmann, D. Lorenz, P. Esser, and B. Ommer. High-resolution image synthesis with latent diffusion models. In *Proceedings of the IEEE/CVF conference on computer vision and pattern recognition*, pages 10684–10695, 2022.
- [22] Y. Rubner, C. Tomasi, and L. J. Guibas. The earth mover’s distance as a metric for image retrieval. *International journal of computer vision*, 40(2):99–121, 2000.
- [23] M. G. Silveri and A. Ocello. Beyond log-concavity and score regularity: Improved convergence bounds for score-based generative models in W2-distance. *ICML*, 2025.
- [24] J. Sohl-Dickstein, E. Weiss, N. Maheswaranathan, and S. Ganguli. Deep unsupervised learning using nonequilibrium thermodynamics. In *ICML*, pages 2256–2265, 2015.

- [25] Y. Song, J. Sohl-Dickstein, D. P. Kingma, A. Kumar, S. Ermon, and B. Poole. Score-based generative modeling through stochastic differential equations. *ICLR*, 2021.
- [26] S. Strasman, A. Ocello, C. Boyer, S. L. Corff, and V. Lemaire. An analysis of the noise schedule for score-based generative models. *TMLR*, 2025.
- [27] P. Vincent. A connection between score matching and denoising autoencoders. *Neural computation*, 23(7):1661–1674, 2011.
- [28] Y. Yu and L. Yu. Advancing wasserstein convergence analysis of score-based models: Insights from discretization and second-order acceleration. *arXiv:2502.04849*, 2025.